## ARTICLE    OPEN

Check for updates

# Changes in temporal inequality of precipitation extremes over China due to anthropogenic forcings

Weili Duan [1,2], Shan Zou[1,2,3 ✉], Nikolaos Christidis [4], Nathalie Schaller[5], Yaning Chen [1 ✉], Netrananda Sahu [6], Zhi Li[1], Gonghuan Fang[1] and Botao Zhou [7]

Based on the Gini-coefficients, this study has presented an analysis of the impacts of anthropogenic forcing on the temporal inequality (i.e., increase in unevenness or disparity) of precipitation amounts (PRCPTOT), intensity (SDII), and extremes (R95p and RX5day) at national and regional scales (eight regions) in China. A positive anthropogenic influence on the temporal inequality is found for precipitation extremes over China, especially in southern regions during the period 1961–2005. Projections of future precipitation indices except R95p have a stepped upward trend in temporal precipitation variability with increasing anthropogenic forcing in most regions of China under SSP126, SSP370, and SSP585 scenarios. Except for Southern China (SC) and SWC2, R95p has a significant decrease in the future, and the largest decrease is up to 29.5% in Northwest China under SSP370. Results obtained from this study offer insights into temporal variability of precipitation extremes and help policy makers for managing water-related disasters.

## INTRODUCTION

Extreme precipitation events have increased in recent decades, which can inevitably be attributed to the combined influence of natural and human activities[1,2], leading to lots of water-related disasters around the world[3]. Examples include heavy flooding in the middle Yangtze River of China in 1998[4], late July-early August 2010 in Pakistan[5], and central Thailand in 2011[6], exceptional drought in the Amazon basin in 2005[7] and 2010[8], and California in 2014[9], causing marked casualties and damage to food systems and social infrastructure. The increase of extreme precipitation events is a prominent phenomenon of precipitation variability, and some studies[9–11] have demonstrated a human influence on precipitation variability. Therefore, it is important to understand and distinguish the extent of the degree of human emissions and activities that have contributed to the climate system and finally affected precipitation variability.

Recent studies about the attribution of extreme weather and climate events indicate that global warming caused by increasing anthropogenic forcings could increase the moisture-holding capacity of the atmosphere potentially, exacerbating the frequency and severity of extreme climate events[12–15]. Some of them show that precipitation variations in spatial distribution directly caused wet regions to become wetter and dry regions drier[16,17], probably because the rising average temperature increases water vapor in the atmosphere, leading to enhanced moisture convergence or divergence in climatologically wet or dry regions[18]. This phenomenon was also found for seasonal precipitation, which means that wet seasons get wetter and dry seasons get drier[19]. However, this argument also has been disputed for changes over land[20–22], revealing large uncertainties in assessments of precipitation variability[23]. One of the

major sources of uncertainty is that the argument did not fully consider the potential changes in interannual or decadal modes of variability with global warming and the teleconnection pathways that linked such changes to the precipitation over land[24]. Some authors have analyzed the temporal behavior of precipitation associated with a warming climate[25,26], including reports of increasing precipitation rates near the tropical cyclone center[27,28], and sensitivity of precipitation extremes to the El Niño variations[29].

Evidence for global warming impacts on the spatiotemporal characteristics of precipitation in China is obvious[30–34]. Based on the global climate model (GCM) outputs in the Coupled Model Intercomparison Project phases 3, 5, and 6 (CMIP3, CMIP5, and CMIP6), most studies suggested more frequency and severe extreme heavy precipitation would happen in China[35,36]. Although some progress has also been made in investigating the impact of anthropogenic forcing on precipitation variability, most of the research focused on trends of mean precipitation and precipitation extremes and can not fully evaluate the uncertainty caused by uncertainty in the model simulations as well as the metrics used to define variability and detect its changes over China[30,33]. To further improve our understanding of potential temporal variability (i.e., increase in unevenness or disparity) in precipitation characteristics associated with a changing climate in China, it is necessary to detect relationships at decadal and longer time scales in order to filter out shorter-term noisy variability in precipitation temporal variability. Thus, in this study, we have evaluated the human contribution to potential changes in temporal inequality of precipitation extremes from 1961 to 2005, and investigated future changes (2061–2095) in temporal inequality of precipitation extremes in China.

[1]State Key Laboratory of Desert and Oasis Ecology, Xinjiang Institute of Ecology and Geography, Chinese Academy of Sciences, Urumqi 830011, China. [2]Akesu National Station of Observation and Research for Oasis Agro-ecosystem, Akesu, Xinjiang 843017, China. [3]Department of Geography, Ghent University, 9000 Ghent, Belgium. [4]Met Office Hadley Centre, Exeter EX1 3PB, United Kingdom. [5]Center for International Climate Research (CICERO), Gaustadalleen 21, 0349 Oslo, Norway. [6]Department of Geography, Delhi School of Economics, University of Delhi, Delhi 110007, India. [7]Collaborative Innovation Center on Forecast and Evaluation of Meteorological Disasters/Key Laboratory of Meteorological Disaster, Ministry of Education, Nanjing University of Information Science and Technology, Nanjing, China. ✉email: zoushan@ms.xjb.ac.cn; chenyn@ms.xjb.ac.cn

## RESULTS

### Evaluation of the present-day simulations

To investigate the influence of anthropogenic forcing on precipitation extremes, the first step is to evaluate GCMs simulation performance for precipitation extreme indices from 1961 to 2005. Results of the evaluation of temporal variation of the present-day simulations for the CMIP5 and CMIP6 GCMs (Supplementary Tables 1 and 2) was shown in Fig. 1 and Table 1. Figure 1a–c compare the Gini-coefficient of the observed distributions and historical simulated distributions (ensemble mean) of precipitation extreme indices from 1961 to 2005, suggesting that both CMIP5 and CMIP6 simulations reasonably captured the magnitudes and spatial patterns of temporal variations for RCPTOT, SDII, R95p, and RX5day (definitions in Supplementary Table 3), which is in line with the results from Konapala et al.[24]. These four indices over China have a distinct regional characteristic, and higher values of the Gini-coefficient were mainly detected in the northwest compared with other regions for CN05 (observed data), CMIP5, and CMIP6. Table 1 shows univariate statistics of the Gini-coefficient of the observed and historical simulated precipitation extreme indices from 1961 to 2005, which indicates that R95p has the highest Gini-coefficient for CN05, CMIP5, and CMIP6, while SDII has the lowest Gini-coefficient. Except for RX5day in CMIP6, the skewness and kurtosis coefficients of precipitation extreme indices are greater than 0, suggesting that distributions of the Gini-coefficient are shifted to the right and more peaked than the normal distribution with the same mean and standard deviation. Moreover, CN05 has higher skewness and kurtosis coefficients than CMIP5 and CMIP6 simulations, which means that the shape of distributions of the Gini-coefficient from CMIP5 and CMIP6 are much closer to normal distributions.

Figure 1 and Table 1 also indicate that the CMIP5 and CMIP6 historical simulations underestimate the Gini-coefficients in most regions of China for all four precipitation indices, especially in Southwest China-region 1 (SWC1, subregions in Supplementary Fig. 1 and Supplementary Table 4) and the Tarim River Basin, while overestimating in a few areas, such as in northern Xinjiang Province. The average bias in percent were −16.52%, −23.86, −18.95, and −17.31% for RCPTOT, SDII, R95p, and RX5day respectively in CMIP5 (Fig. 1f), and increased to −6.86, −15.02, −14.33, and −8.01% in CMIP6, which suggests that CMIP6 has a better performance in simulations of precipitation extremes in this study. For both CMIP5 and CMIP6, SDII has the largest bias, while RX5day has the lowest bias. Generally, the areas with high bias in the Gini-coefficient of precipitation indices have sparse meteorological stations (Supplementary Fig. 1) or have high altitudes (such as SWC1), where the GCM simulations have a general weakness in rainfall prediction[37].

Overall, although the simulations of CMIP5 and CMIP6 underestimate the observed Gini-coefficients in some regions, they can generally capture the spatial patterns of the annually observed precipitation variability in China and could be used to quantify the anthropogenic contribution to changes in the temporal variability of RCPTOT, SDII, R95p, and RX5day.

### Temporal variability of precipitation due to anthropogenic forcings

A positive shift in the probability distributions of the averaged bootstrap resampled Gini-coefficients has been detected for all precipitation indices from CMIP5 NAT to ALL scenarios (Fig. 2a–d), and the value of the median Gini-coefficient increased from 0.101 to 0.103 for PRCPTOT, 0.066 to 0.067 for SDII, 0.268 to 0.271 for R95p, and 0.142 to 0.144 for RX5day. Of them, except for RX5day ($p = 0.19$), changes from the other three precipitation indices are statistically significant ($p < 0.01$). Figure 2e–h shows the probability distributions, the median, and 95th percentile

values of the relative anthropogenic index (RAI, see methods for details), which are calculated from all the resampled Gini-coefficients. There is an increase in RAI for PRCPTOT (0.012), SDII (0.015), R95p (0.007), and RX5day (0.004), suggesting much higher temporal variability due to anthropogenic contributions over China during the period 1961–2005. However, Fig. 2b also shows that the fifth percentile values of the RAI (see dashed line) are less than zero, revealing that the decrease is not statistically significant in uniformity (i.e., increase in unevenness or disparity) of PRCPTOT, SDII, R95p and RX5day by 1.2, 1.5, 7, and 4%, respectively due to anthropogenic forcings.

Except for R95p in the NEC region, the median averaged Gini-coefficient of ALL scenario was greater than the value of the NAT scenario for all precipitation indices in eight regions (Fig. 2i–l), indicating human contribution to potential changes in temporal precipitation variability over China. A similar distribution has been found in PRCPTOT, SDII, and R95p in eight regions; of them, NWC has the highest values of the median averaged Gini-coefficient, followed by NC and NEC, revealing that a relatively higher temporal precipitation variability for PRCPTOT, SDII, and R95p in these regions. For RX5day, NC has the highest values of the median averaged Gini-coefficient, followed by NWC, NEC, and SC, revealing a relatively higher temporal precipitation variability for RX5day in these regions. Figure 2i–l also indicates that SWC1 has the lowest values of the median averaged Gini-coefficient for both ALL and NAT scenarios, illustrating a relatively lower temporal precipitation variability for all four precipitation indices in Qinghai-Tibet regions. Generally, regardless of CMIP5 ALL or NAT scenarios, the resampled averaged Gini-coefficients of northern China (NWC, NC, and NEC) are higher than that of southern China. The possible reasons for this phenomenon are first because there are less precipitation frequency and precipitation amounts in northern China than in southern China, and secondly, because there are more rainy months in southern China than in northern China[38,39]. All these reasons generally make the precipitation distribution in southern China relatively even.

Figure 3 indicates the best RAI estimates in eight regions of China along with their uncertainty range at 95 and 5% limits (maximum and minimum values), which reveals that generally, the best RAI estimates in southern China is higher than in the north, suggesting the higher anthropogenic influence on the variability of four precipitation indices in southern China. The influence is generally reflected by the changes in severe weather phenomena (e.g., Meiyu rainband, tropical cyclones). For example, the increase of tropical cyclones (TCs) contributes significantly to an upward trend of rainfall intensity in summer and autumn in southern China[40], and an increasing trend in SDII, R95p, and RX5day over southeastern China and the Meiyu rainband, suggesting that extreme precipitation rates will be likely to enhance in future[41]. Among all eight regions, the SWC2 region exhibits the highest anthropogenic influence on the variability of PRCPTOT, SDII, R95p, and RX5day, the best RAI estimates of which are 0.0674, 0.0546, 0.0424, and 0.0404, respectively. Meanwhile, based on the value of the 5% limit, there is a statistically significant (95% confidence) increase in nonuniformity of PRCPTOT, SDII, and RX5day by 6.74, 5.46, and 4.04% respectively in the SWC2 region due to anthropogenic forcing. The finding could be used to explain why there were more severe precipitation anomalies (e.g., extreme dry events) in Yunnan province in recent years[42]. Also, the NWC region has the lowest best RAI estimates for PRCPTOT, SDII, R95p, and RX5day, suggesting a statistically insignificant decrease in nonuniformity of PRCPTOT, SDII, R95p, and RX5day by 8.37, 1.80, 1.04, and 2.17% due to anthropogenic forcing. This is consistent with the results obtained from a study[43] that discovered a decrease in the temporal inequality of precipitation in arid regions of China with the increase in air temperature. Under global warming, heavy precipitation amount dominated by the frequency-enhanced rainstorms increased gradually in the
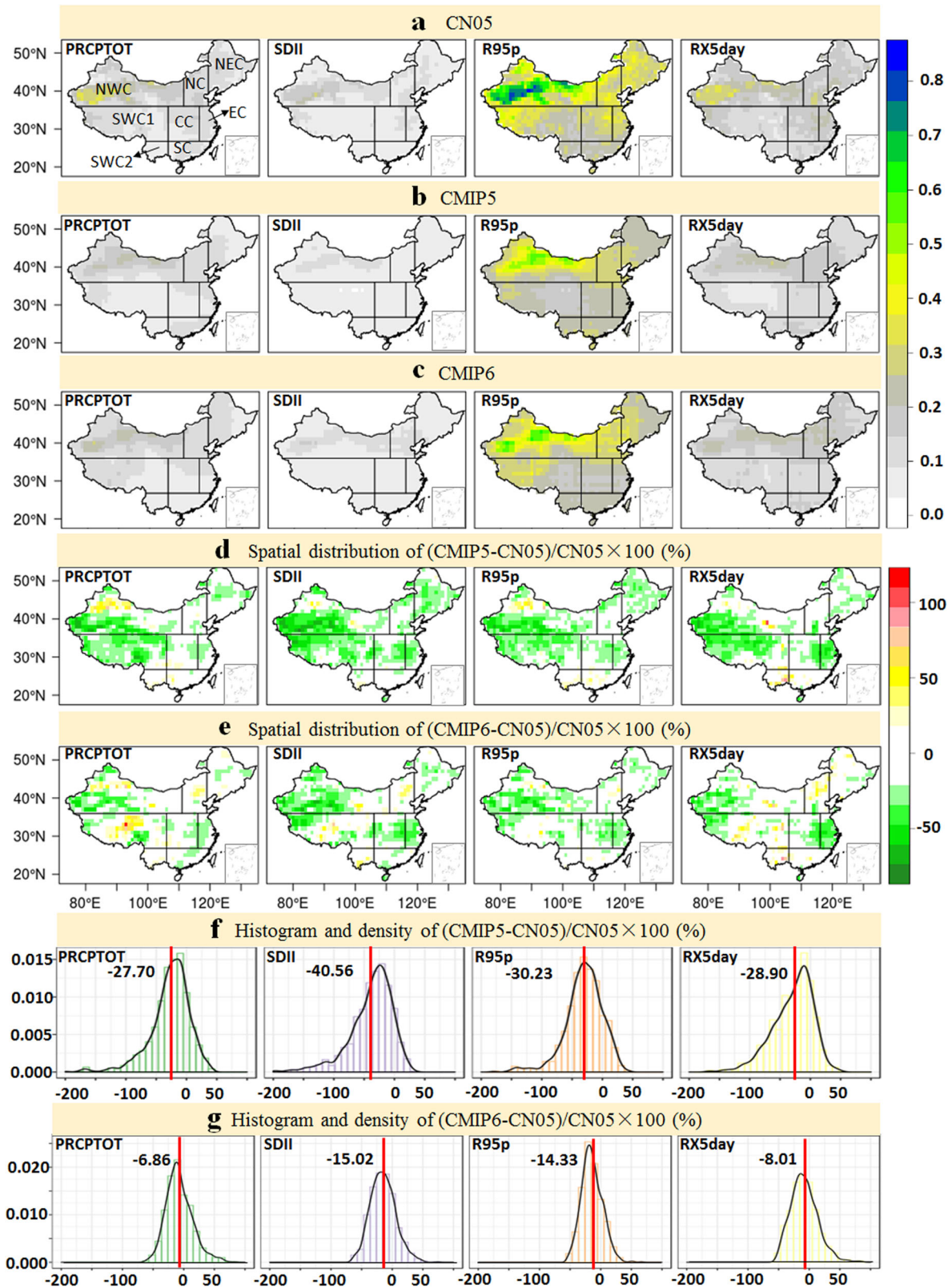
**Fig. 1  Comparison of Gini-coefficients between observed and simulated values.** Gini-coefficients at spatial distributions of **a** CN05 dataset, **b** CMIP5 historical simulations, **c** CMIP6 historical simulations, **d** the bias [(CMIP5-CN05)/CN05] (%), **e** the bias [(CMIP6-CN05)/CN05] (%), **f** histogram and density plots of the bias [(CMIP5-CN05)/CN05] (%), and **g** histogram and density plots of the bias [(CMIP6-CN05)/CN05] (%)for four indices from 1961 to 2005. Red lines are the average value for all grids. The subfigures were done in the software R 4.0.2 (https://cran.r-project.org/bin/windows/), and then the subfigures were merged by using the Microsoft PowerPoint 2013 software (https://www.microsoft.com/).

**Table 1.** Univariate statistics of the Gini-coefficient of the observed and historical simulated precipitation extreme indices from 1961 to 2005.

| Data | Indices | Mean | SD | Maximum | Minimum | Skewness | Kurtosis |
|------|---------|------|------|---------|---------|----------|----------|
| CN05 | PRCPTOT | 0.13 | 0.06 | 0.35 | 0.05 | 1.66 | 2.7 |
| | SDII | 0.09 | 0.03 | 0.27 | 0.04 | 1.84 | 3.91 |
| | R95p | 0.34 | 0.13 | 0.82 | 0.16 | 1.52 | 1.80 |
| | RX5day | 0.17 | 0.05 | 0.35 | 0.07 | 0.83 | 0.74 |
| CMIP5 | PRCPTOT | 0.10 | 0.04 | 0.22 | 0.04 | 1.26 | 1.49 |
| | SDII | 0.06 | 0.02 | 0.14 | 0.03 | 1.11 | 1.53 |
| | R95p | 0.27 | 0.08 | 0.57 | 0.24 | 1.68 | 2.56 |
| | RX5day | 0.14 | 0.03 | 0.26 | 0.06 | 0.37 | 0.56 |
| CMIP6 | PRCPTOT | 0.11 | 0.04 | 0.27 | 0.05 | 1.18 | 1.44 |
| | SDII | 0.07 | 0.02 | 0.17 | 0.04 | 1.36 | 1.84 |
| | R95p | 0.28 | 0.08 | 0.63 | 0.16 | 1.54 | 2.54 |
| | RX5day | 0.15 | 0.03 | 0.25 | 0.08 | 0.72 | −0.18 |

northern and inner parts of China[44], possibly reflecting the decrease in RAI estimates in NWC.

## Temporal variability of precipitation in future

The distributions of the Gini-coefficient of historical simulations (1961–2005) and CMIP6 future simulations (SSP126, SSP370, and SSP585 from 2051 to 2095) for four precipitation indices are illustrated in Fig. 4 and show that future simulations have similar distributions like historical simulations over China, suggesting that the values in northern China are generally higher than that in southern regions. These distributions also reflect more precipitation amounts and frequency in the south than that in the north. The largest Gini-coefficient of PRCPTOT for three future scenarios are detected in Xinjiang and Inner Mongolia Provinces, up to 0.25, while the lowest Gini-coefficient is found in the southwestern region, close to zero. Figure 4a also indicates that a negative change is found in NWC (especially in Xinjiang Province) and northern SWC1, while a positive change in southwestern and central regions for all three scenarios, and the change ranges from −20 to 30%. PRCPTOT projections under SSP370 are almost equivalent to the projections under SSP585, with a positive change in small regions of southwestern China. Similar to PRCPTOT, SDII has a positive change in Xinjiang Province and a positive change in southwestern and northeastern regions under all three scenarios, with a range from −30 to 40%.

The largest Gini-coefficient for R95p and RX5day is up to 0.60 and 0.25, respectively, which are detected in the southern flank of northwest China (Fig. 4c, d). Meanwhile, Fig. 4c also indicates that the Gini-coefficient of R95p projections under all three SSPs is less than those in historical simulations in most regions of China, especially in the northwest region, which is similar to the comparison between CMIP5 ALL and NAT simulations in Fig. 3. Due to the semi-arid and arid climate, the annual precipitation in Northwest China is less than 200 mm with an increasing trend in extreme precipitation events since 1961[44], possibly reflecting the decrease in Gini estimates across this region in the future. In contrast, most of the regions in China show a positive bias for RX5day under all three scenarios, and the largest bias is detected in the Qinghai-Tibet region, up to 60% (Fig. 4d). Also, Fig. 4d shows that RX5day projections under SSP585 are almost equivalent to the projections in most regions of China under SSP370.

Except for R95p, a positive shift has been detected for the other three precipitation indices under three scenarios, suggesting an increase in Gini-coefficients under future SSP370 and SSP585 simulations (Fig. 5). Moreover, under the SSP585 scenario, the value of the median value over China increases to 0.113, 0.075,

and 0.158 for PRCPTOT, SDII, and RX5day, respectively (Table 2). In contrast, the value of the median Gini-coefficient for R95p decreases from 0.278 to 0.248, 0.241, and 0.241 for SSP126, SSP370, and SSP585 scenarios, respectively. These results indicate that there will likely be more and more precipitation events, contributing to the temporal inequality (i.e., an increase in unevenness or disparity). Figure 5e–h show the probability distributions, the median, and 95th percentile values (or fifth percentile values) of the relative future index (RFI, see methods for details) for three future scenarios, which indicates that there is an increase in RFI for PRCPTOT, SDII, and RX5day under three future scenarios, with the exception of R95p. Furthermore, a statistically significant increase in RFI is found for SDII, and RX5day for both SSP370 and SSP585 scenarios, the value of which are 0.052 and 0.070 and 0.036 and 0.054, respectively. The results show much higher temporal variability in daily intensity index and max 5-day precipitation amount due to increasing anthropogenic forcings under SSP370 and SSP585 scenarios in the future over China, and the corresponding rate of change are 5.2 and 7% and 3.6 and 5.4%, respectively. On the contrary, a statistically significant decrease in RFI is found for R95p under SSP126, SSP370, and SSP585 scenarios, suggesting a lower temporal variability due to increasing anthropogenic forcings in the future over China, with the corresponding rate of change at −13.2, −15.9, and −15.6%, respectively.

The resampled averaged Gini-coefficients of four precipitation indices have similar characteristics in eight regions for PRCPTOT, SDII, and RX5day (Fig. 6). Of them, except for NWC, NC, and NEC, the Gini-coefficients of these three precipitation indices are all projected to increase in the 21st century, suggesting an increasing trend in temporal precipitation variability in the future. For R95p, generally, historical simulations have higher median Gini-coefficients than those in future simulations in most regions with the exception of SC and SWC2. Also, whether it is historical or future simulations, R95p has the highest median Gini-coefficients in eight regions, followed by RX5day, PRCPTOT, and SDII, which indicates the largest temporal inequality in R95p in the future. Moreover, NWC has the highest median Gini-coefficients of R95p for SSP126, SSP370, and SSP585 simulations, with the corresponding value at 0.310, 0.285, and 0.285, respectively (Table 2), illustrating that a relatively higher temporal precipitation variability for R95p in future.

Figure 7 shows the best RFI estimates in eight regions of China along with their uncertainty range at 95 and 5% limits (maximum and minimum values) for future simulations, which reveals that generally, the best RFI estimate in the south of China is higher than the north for precipitation indices, suggesting the higher anthropogenic influence on the temporal variability in southern China. Overall, projections of PRCPTOT, SDII, and RX5day have
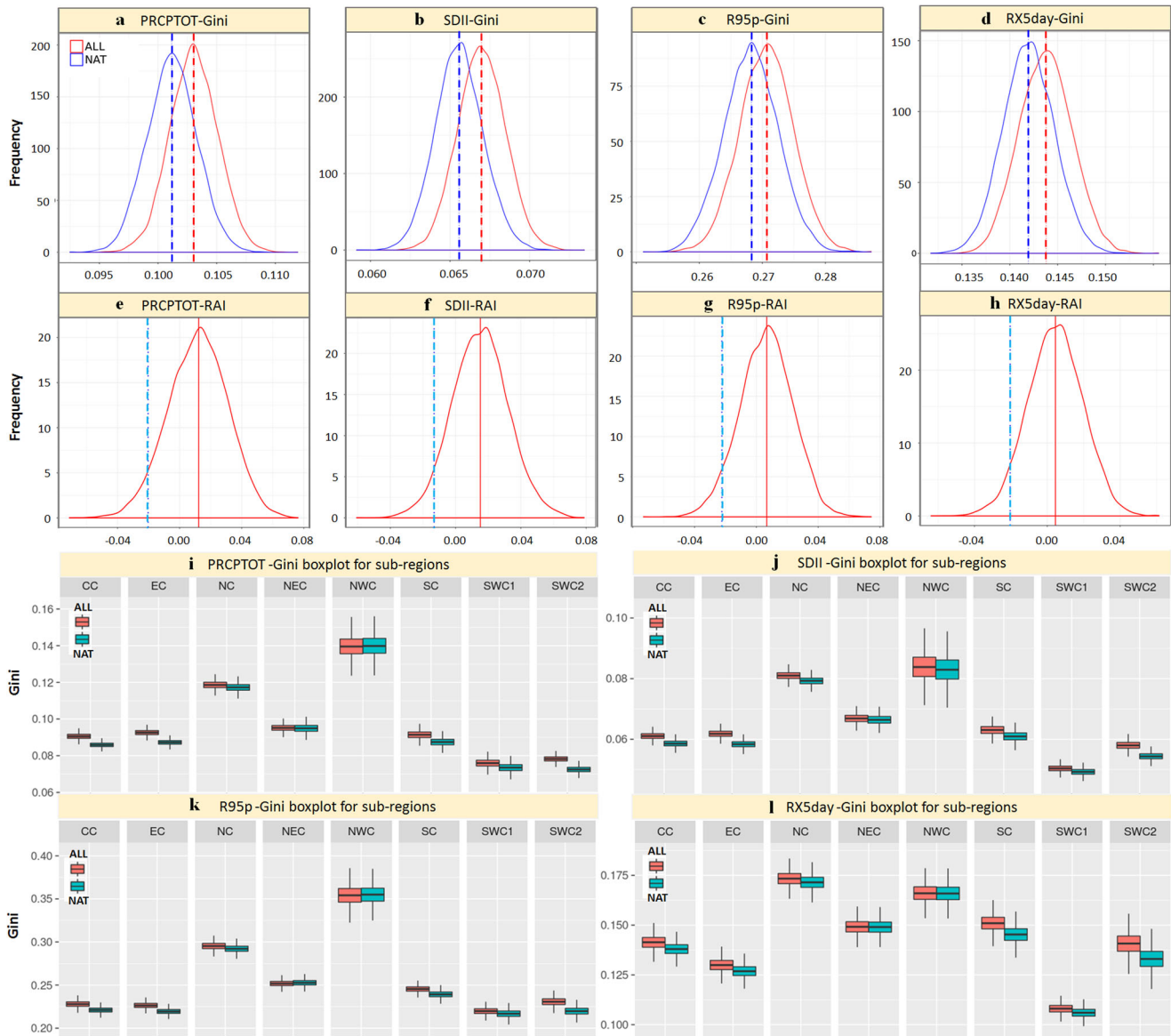
**Fig. 2 Maps of the resampled averaged Gini-coefficients and RAI. a–d** The probability distribution functions of the resampled averaged Gini-coefficients for four precipitation extreme indices over China for CMIP5 ALL and NAT scenarios obtained by the bootstrapping procedure and the dashed line indicates the median (best estimate) value of Gini-coefficients. **e–h** The probability distribution functions of RAI values over China, and the solid red line indicates the median (best estimate) value of RAI, and the dashed line indicates the fifth percentile value; the **i–l** subfigures are the boxplots of the resampled averaged Gini-coefficients for eight subregions. The subfigures were done in the software R 4.0.2 (https://cran.r-project.org/bin/windows/) and then the subfigures were merged by using the Microsoft PowerPoint 2013 software (https://www.microsoft.com/).

similar features in eight regions, showing a stepped upward trend in most regions between SSP126, SSP370, and SSP585 simulations. For PRCPTOT projections, the best RFI is greater than zero in most regions under SSP370 and SSP585 scenarios, while less than zero in most regions under the SSP126 scenario. Of them, the best RFI value in CC, EC, SC, SWC1, and SWC2 regions indicate a statistically significant (95% confidence) change under both SSP370 and SSP585 simulations, which suggests that the temporal variability of annual precipitation is likely to increase due to anthropogenic forcing by 5.0 and 8.1% in CC, 4.7 and 6.2% in EC, 8.7 and 8.5% in SC, 3.1 and 6.6% in SWC1, and 13.1 and 14.6% in SWC2. And no matter what emission scenario exists, the RFI values for NWC and NC are less than zero for PRCPTOT, with a statistically significant decrease in temporal variability for all three future simulations.

The best RFI estimates for SDII are significantly greater than zero in SC, SWC1, and SWC2 for all three future scenarios (Fig. 7c, d), suggesting a significant increase in temporal variability in the averaged wet day daily amount (SDII) in these regions. Under SSP585, the largest best RFI is found in SWC2 (0.201), followed by SC (0.161) and SWC1 (0.135), which indicate that there is a statistically significant (95% confidence) increase in nonuniformity of SDII by 20.1% in SWC2, 16.1% in CC, and 13.5% in SC. Similar to PRCPTOT, the RFI value in NWC is significantly less than zero for SDII for all three future scenarios, suggesting a statistically significant (95% confidence) decrease in nonuniformity of SDII by 6.0%, 6.0, and 3.3% for SSP126, SSP370, and SSP585 scenarios, respectively in this region.

Similarly, exception of NC and NWC, the best RFI estimates for RX5day are significantly greater than zero over China under
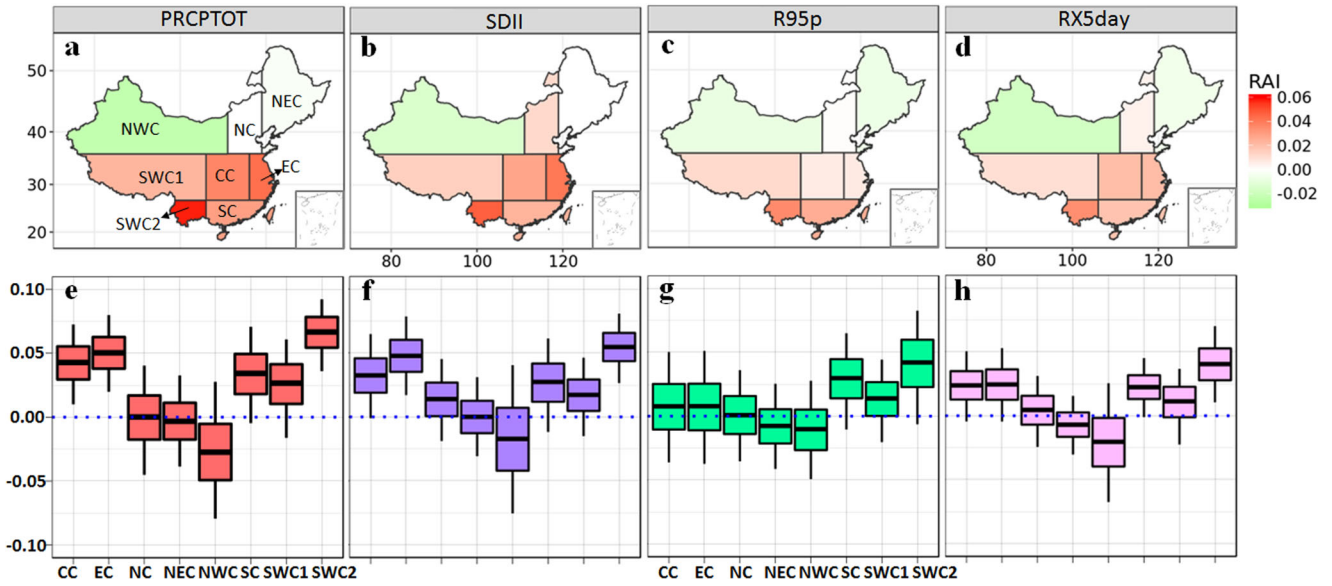
**Fig. 3 Maps of the RAI estimates. a–d** The best temporal RAI estimates over eight regions in China for PRCPTOT (mm/year), SDII (mm/day), R95p (mm), and RX5day (mm) respectively. **e–h** The uncertainty range (5th to 95th percentile) of RAI and the horizontal line in the box represents the best estimate (i.e., median value). The subfigures were done in the software R 4.0.2 (https://cran.r-project.org/bin/windows/), and then the subfigures were merged by using the Microsoft PowerPoint 2013 software (https://www.microsoft.com/).
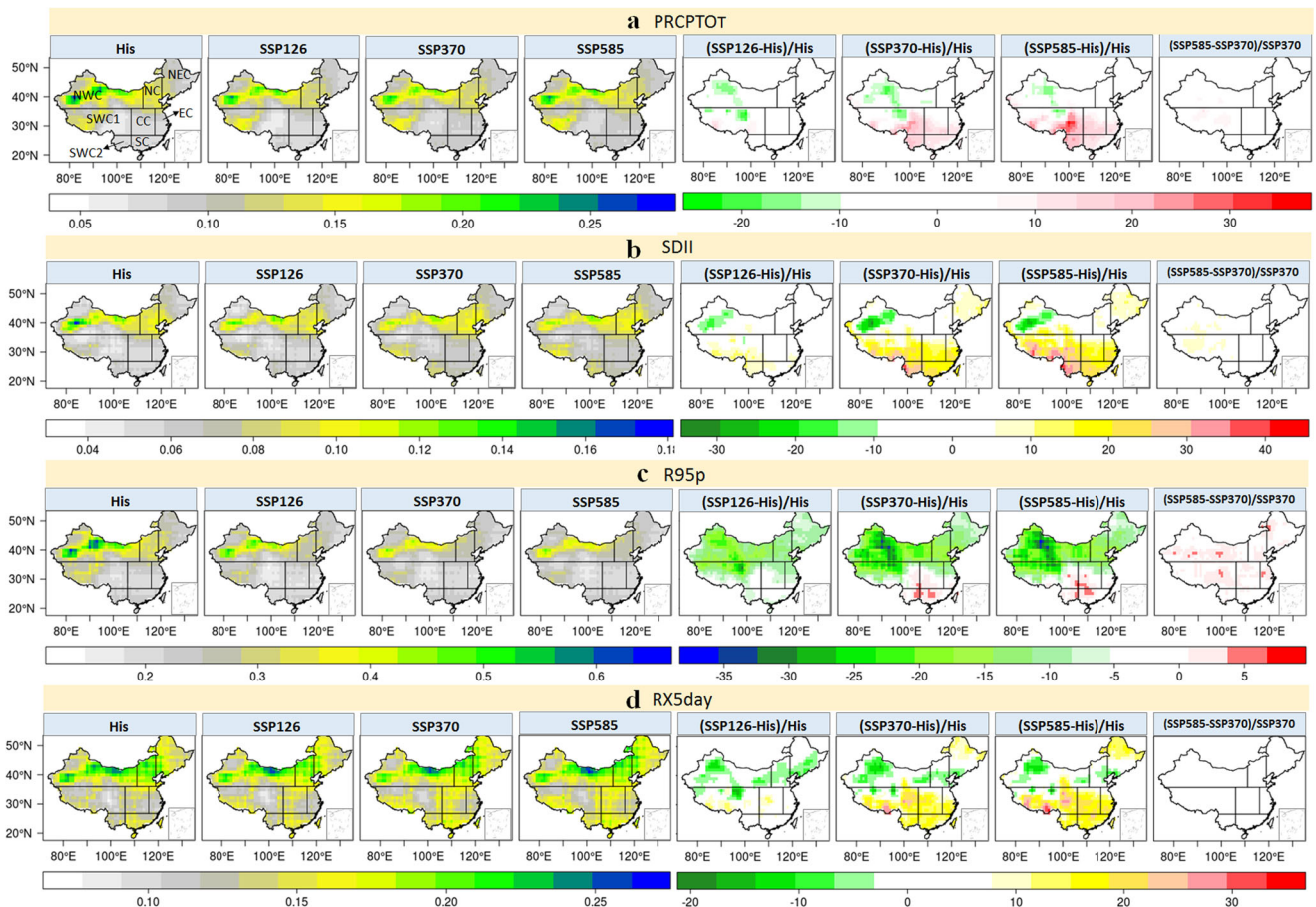


**Fig. 4 Comparison of Gini-coefficients between historical and future simulations.** Comparison between historical simulations (1961–2005) and future simulations (SSP126, SSP370, and SSP585, from 2051 to 2095) Gini-coefficients for **a** PRCPTOT, **b** SDII, **c** R95p, and **d** RX5day. The subfigures were done in the software R 4.0.2 (https://cran.r-project.org/bin/windows/), and then the subfigures were merged by using the Microsoft PowerPoint 2013 software (https://www.microsoft.com/).
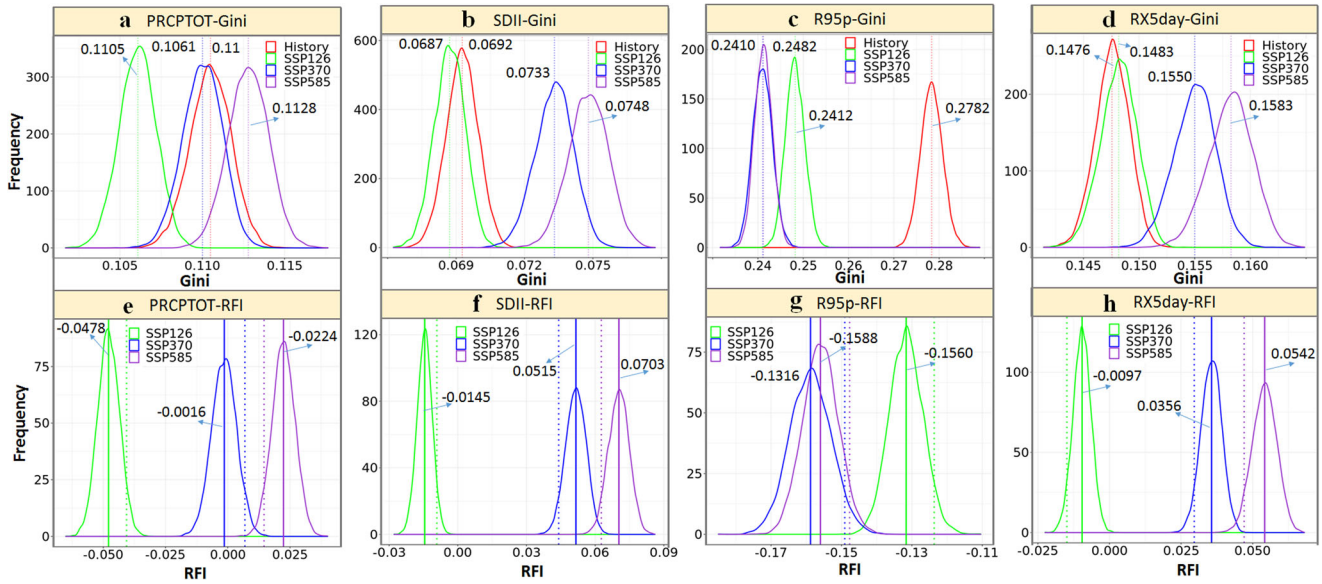
**Fig. 5 Maps of the resampled averaged and median (best estimate) Gini-coefficients.** The figure on the top panel represents the probability distribution functions of the resampled averaged Gini-coefficients for **a** PRCPTOT, **b** SDII, **c** R95p, and **d** RX5day over China for historical simulations (1961–2005) and future simulations (SSP126, SSP370, and SSP585, from 2051 to 2095), and the dashed line indicates the median (best estimate) value of Gini-coefficients. The bottom panel indicates the probability distribution functions of RFI values for **e** PRCPTOT, **f** SDII, **g** R95p, and **h** RX5day over China as obtained from utilizing the CMIP6 historical and future simulations from the top panels, and the solid straight line indicates the median (best estimate) value of RFI and the dashed line straight indicates the 95th percentile value or 5th percentile value. The subfigures were done in the software R 4.0.2 (https://cran.r-project.org/bin/windows/), and then the subfigures were merged by using the Microsoft PowerPoint 2013 software (https://www.microsoft.com/).

| Table 2. | Medium values of Gini in eight subregions and the whole of China for historical and future simulations. | | | | | | | | |
|---|---|---|---|---|---|---|---|---|---|
| Regions | Scenarios | NEC | NC | EC | CC | SC | SWC1 | SWC2 | NWC | China |
| PRCPTOT | His | 0.100 | 0.132 | 0.088 | 0.087 | 0.080 | 0.097 | 0.080 | 0.148 | 0.110 |
| | SSP126 | 0.095 | 0.124 | 0.087 | 0.086 | 0.081 | 0.096 | 0.083 | 0.137 | 0.106 |
| | SSP370 | 0.101 | 0.127 | 0.094 | 0.093 | 0.089 | 0.101 | 0.094 | 0.136 | 0.110 |
| | SSP585 | 0.101 | 0.129 | 0.095 | 0.095 | 0.089 | 0.105 | 0.096 | 0.141 | 0.113 |
| SDII | His | 0.070 | 0.092 | 0.059 | 0.061 | 0.057 | 0.058 | 0.061 | 0.084 | 0.069 |
| | SSP126 | 0.069 | 0.090 | 0.060 | 0.061 | 0.060 | 0.060 | 0.066 | 0.079 | 0.069 |
| | SSP370 | 0.075 | 0.094 | 0.067 | 0.067 | 0.069 | 0.066 | 0.077 | 0.078 | 0.073 |
| | SSP585 | 0.075 | 0.095 | 0.068 | 0.068 | 0.070 | 0.068 | 0.079 | 0.080 | 0.075 |
| R95p | His | 0.261 | 0.312 | 0.217 | 0.218 | 0.221 | 0.250 | 0.215 | 0.363 | 0.278 |
| | SSP126 | 0.238 | 0.278 | 0.200 | 0.204 | 0.212 | 0.222 | 0.205 | 0.310 | 0.248 |
| | SSP370 | 0.235 | 0.267 | 0.202 | 0.208 | 0.224 | 0.219 | 0.217 | 0.285 | 0.241 |
| | SSP585 | 0.235 | 0.267 | 0.203 | 0.208 | 0.222 | 0.220 | 0.217 | 0.285 | 0.241 |
| RX5day | His | 0.158 | 0.193 | 0.122 | 0.131 | 0.140 | 0.121 | 0.129 | 0.169 | 0.148 |
| | SSP126 | 0.156 | 0.186 | 0.126 | 0.139 | 0.145 | 0.125 | 0.131 | 0.165 | 0.148 |
| | SSP370 | 0.166 | 0.189 | 0.134 | 0.148 | 0.160 | 0.134 | 0.146 | 0.165 | 0.155 |
| | SSP585 | 0.169 | 0.192 | 0.138 | 0.152 | 0.163 | 0.137 | 0.147 | 0.169 | 0.158 |

SSP370 and SSP585 scenarios (Fig. 7), suggesting a significant increase in temporal variability in the annual maximum 5-day precipitation (RX5day) in these regions. Under the SSP585 scenario, the largest best RFI is found in SC (0.120), followed by SWC2 (0.119) and CC (0.114), which indicate that there is a statistically significant increase in nonuniformity of RX5day by 12.0% in SC, 11.9% in SWC2, and 11.4% in CC. On the contrary, the best RFI estimates for RX5day are significantly less than zero in NC and NWC for all three future scenarios (Fig. 7), suggesting a significant decrease in temporal variability in the averaged wet day daily amount (SDII). Of them, the lowest best

RFI is found for the SSP126 scenario in NC (−0.047), which indicates that there is a statistically significant decrease in nonuniformity of RX5day by 4.7% in NC under a very low forcing level. Except for SC and SWC2 under SSP370 and SSP585 scenarios, the best RFI estimates for R95p are significantly less than zero over China in the future (Fig. 7), indicating a significant decrease in temporal variability of the annual total precipitation on very wet days (R95p) in future. Of them, the smallest best RFI was found in NWC under the SSP370 scenario, the value of which is up to −0.295, suggesting a statistically significant decrease in nonuniformity of R95p by 29.5%.
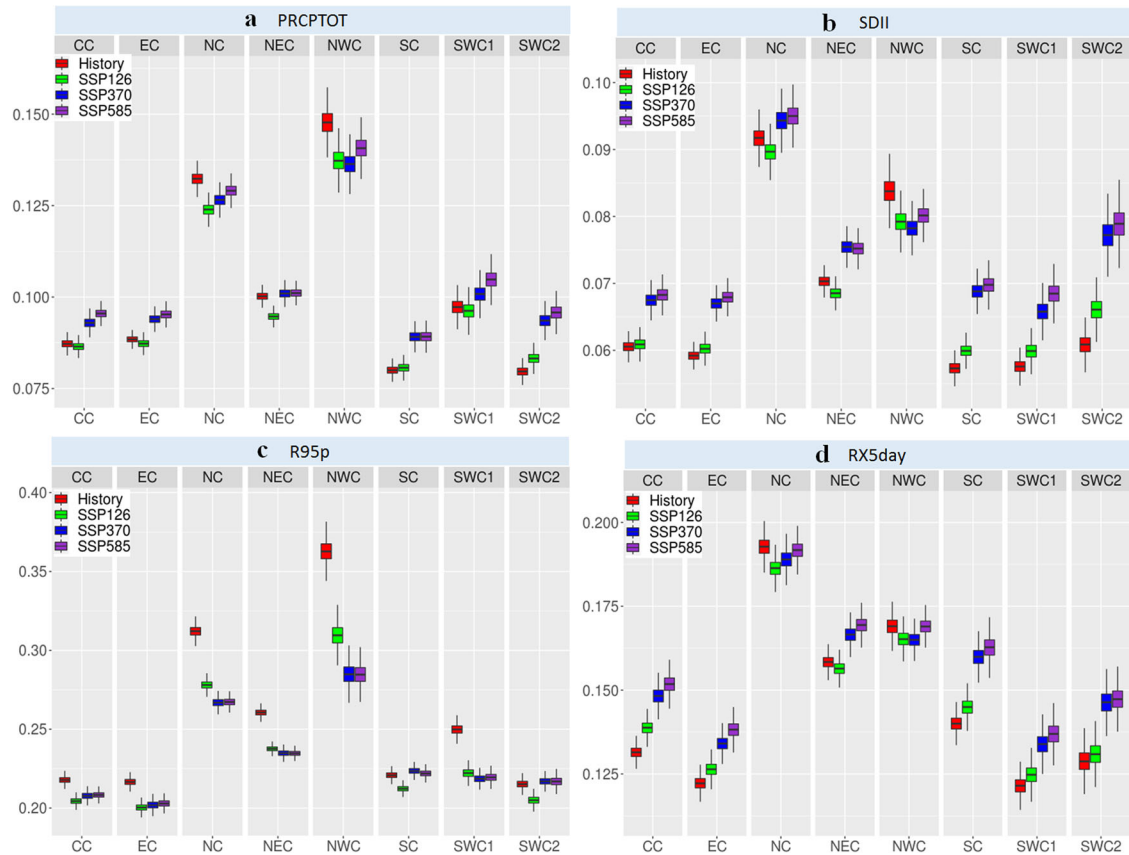
**Fig. 6   Boxplots of the resampled averaged Gini-coefficients in eight regions.** Boxplots for **a** PRCPTOT, **b** SDII, **c** R95p, and **d** RX5day for eight regions in China for CMIP6 for historical simulations (1961–2005) and future simulations (SSP126, SSP370, and SSP585, from 2051 to 2095) obtained by the bootstrapping procedure. The subfigures were done in the software R 4.0.2 (https://cran.r-project.org/bin/windows/), and then the subfigures were merged by using the Microsoft PowerPoint 2013 software (https://www.microsoft.com/).

## DISCUSSION

Both CMIP5 and CMIP6 simulations underestimate the Gini-coefficients in most regions of China, especially in Northwest China, where there are sparse meteorological stations. This kind of underestimation has been also found by Konapala et al.[24], which may reflect the general weakness of rainfall prediction in GCM simulations because the topography is the main influencing factor that force precipitation patterns[37]. Another reason is that the accuracy of the observed CN05 data were also affected by the number of meteorological observation station in different regions, the bias of which could be large in these regions with sparse stations. However, results from the evaluation of temporal variation of the present-day simulations for CMIP5 and CMIP6 historical simulations can generally capture the magnitudes and spatial patterns of temporal variations for RCPTOT, SDII, R95p, and RX5day, which are consistent with the results of previous studies[36,45]. Moreover, CMIP6 generally performs better than CMIP5 in historical simulations of precipitation extremes.

A clear signal indicating a positive anthropogenic influence on the temporal variability of PRCPTOT, SDII, R95p, and RX5day over China by comparing CMIP5 ALL and NAT simulations, suggesting an increase in nonuniformity (i.e., decrease in unevenness) in annual precipitation amount and intensity. The result is consistent with the finding of Li et al.[33], and they argued that anthropogenic forcings are likely to partially drive the intensification of extreme precipitation over China. Meanwhile, it is very difficult to clearly recognize the anthropogenic aerosol effect in current models, and both aerosol–cloud interactions and aerosol–radiation interactions can influence extreme precipitation over China[46]. Compared to

northern China, a higher anthropogenic influence on the variability was found for four precipitation indices in southern China, which is consistent with the findings of previous studies (e.g., Sun et al.[43]) that documented an increased contribution to the overall precipitation amount from extreme events and higher temporal inequality of precipitation in southeastern China with global warming, but a decrease in the temporal inequality of precipitation in northern China, especially in arid regions. The possible reason for this phenomenon is that both precipitation frequency and precipitation amounts in arid regions are inherently scarce. Within a certain range, an increase in precipitation frequency will improve the uniformity (i.e., decrease in uneven-ness) in annual precipitation amount and intensity, but at the same time, it will increase the risk of precipitation extremes (i.e., the increase of RX5day).

In addition, why the SWC2 region exhibits the highest anthropogenic influence on the temporal variability of PRCPTOT, SDII, R95p, and RX5day? SWC2 region mainly contains the Yunnan Province, which is a sensitive region for climate change due to its geographic and ecological background, and is strongly influenced by the South Asian monsoon (SAM), East Asian monsoon (EAM), and air masses from the Qinghai-Tibet Plateau[47]. With global warming, the index of EAM and SAM has been confirmed to decrease in the recent decades, and its fluctuation is becoming more frequent, which contributed to severe precipitation anomalies[42,48], increasing the probability of concurrent extreme wet and dry events for Yunnan[49].

Also, in the past decades, human activities, such as burning fossil fuels, have significantly contributed to global warming, which probably affects the atmospheric circulation, eventually
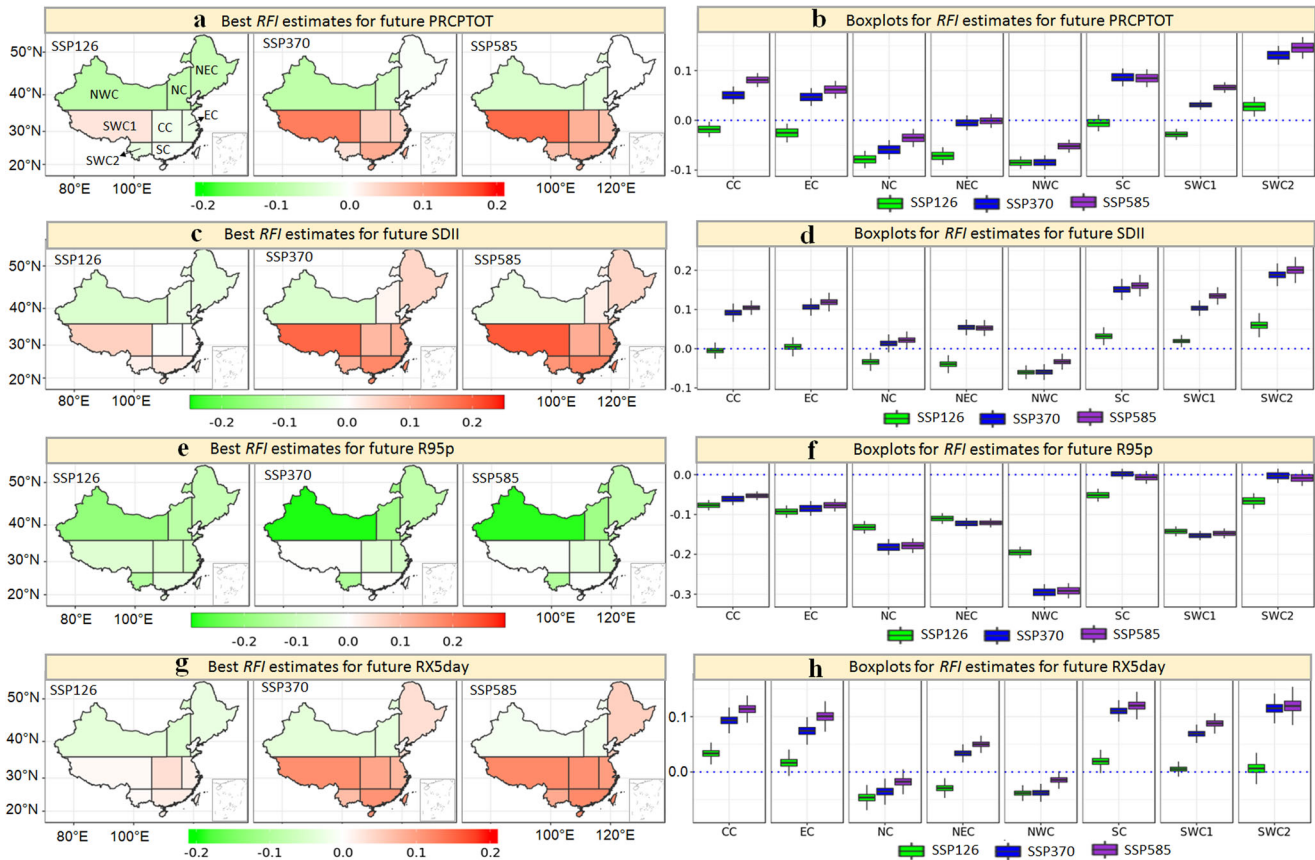
**Fig. 7  Maps of the best temporal RFI estimates.** The best temporal RFI estimates were calculated based on the bootstrapping procedure for **a** PRCPTOT, **c** SDII, **e** R95p, and **g** RX5day over eight regions in China. **b, d, f, h** The uncertainty range (5th to 95th percentile) of RFI and the horizontal line in the box represents the best estimate (i.e., median value). The subfigures were done in the software R 4.0.2 (https://cran.r-project.org/bin/windows/) and then the subfigures were merged by using the Microsoft PowerPoint 2013 software (https://www.microsoft.com/).

causing temporal variability of precipitation (i.e., increase of precipitation extremes)[50,51]. To investigate the characteristics of the temporal variability of precipitation in China, the composite analysis was performed based on the following atmospheric variables in the data of the NCEP/NCAR Reanalysis 1: air temperature, geopotential height, and wind at 500 hPa, and specific humidity from 300 to 1000 hPa. Generally, an increasing trend in the air temperature and geopotential height at 500 hPa was found over China, especially in northwestern regions (Fig. 8a, b). The increasing trend in temperature plays a role in holding more water vapor, probably increasing the risk of extreme precipitation events[52,53]. An increasing trend in specific humidity was detected in most regions of western China (e.g., northern Xinjiang and Tibet), which may contribute to wetter in these regions[54,55]. Also, an anomalous anticyclonic circulation was found over Mongolia and northern China (Fig. 8d) in the later period (1991–2018), which probably favored the divergence of water vapor (Fig. 8d shows that the increasing westerly winds (about 2 m s$^{-1}$) brought more water vapor from the Atlantic Ocean and the increasing easterly winds brought more water vapor from the Sea of Okhotsk and the western Pacific) under an increasing humidity (Fig. 8c) and increased the frequency of precipitation extremes in these regions. Generally, climate warming induced by anthropogenic forcing under CMIP5 ALL simulations has been proved to significantly affect both thermodynamic and dynamic mechanisms, and eventually change the atmospheric circulation[56]. For the future atmospheric circulation changes under global warming, Chen[57] indicated that the East Asian summer monsoon circulation has been projected to be considerably stronger, and

the local atmospheric stratification has been projected to be more unstable, all of which provide a background benefit for the increase of extreme precipitation events in China.

Finally, why R95p has a significant decrease in temporal variability in most regions of China under SSP126, SSP370, and SSP585 simulations? Some previous studies[27,36] have already demonstrated that human-induced increases in greenhouse gases will possibly contribute to the heavy precipitation events (i.e., more flooding) over China, especially under the SSP585 scenario. The value of R95p could be increased in the future[36], but its temporal variability may get weaker in the future than in the historical simulations in northwestern China. It may be because the percentage increase in R95p is larger than that of PRCPTOT, which indicates that an increase in precipitation falling on very wet days has a larger contribution to the total precipitation change[36], and this appropriate increase in frequency will tend to cause a uniform distribution for R95p in future. In this study, the Gini-coefficients of R95p in northern China (especially in Xinjiang Province) are much higher than those in the southwestern region, and future Gini-coefficients are basically less than the historical ones in these regions. Of course, although the CMIP5 and CMIP6 GCMs provide a powerful tool to evaluate impacts from anthropogenic forcings on precipitation extremes and predicate temporal variability of precipitation extremes in the future, further work is needed to more precisely quantify the fraction of risk attributable to anthropogenic and natural factors at the regional scale, especially in these regions with sparse meteorological stations.
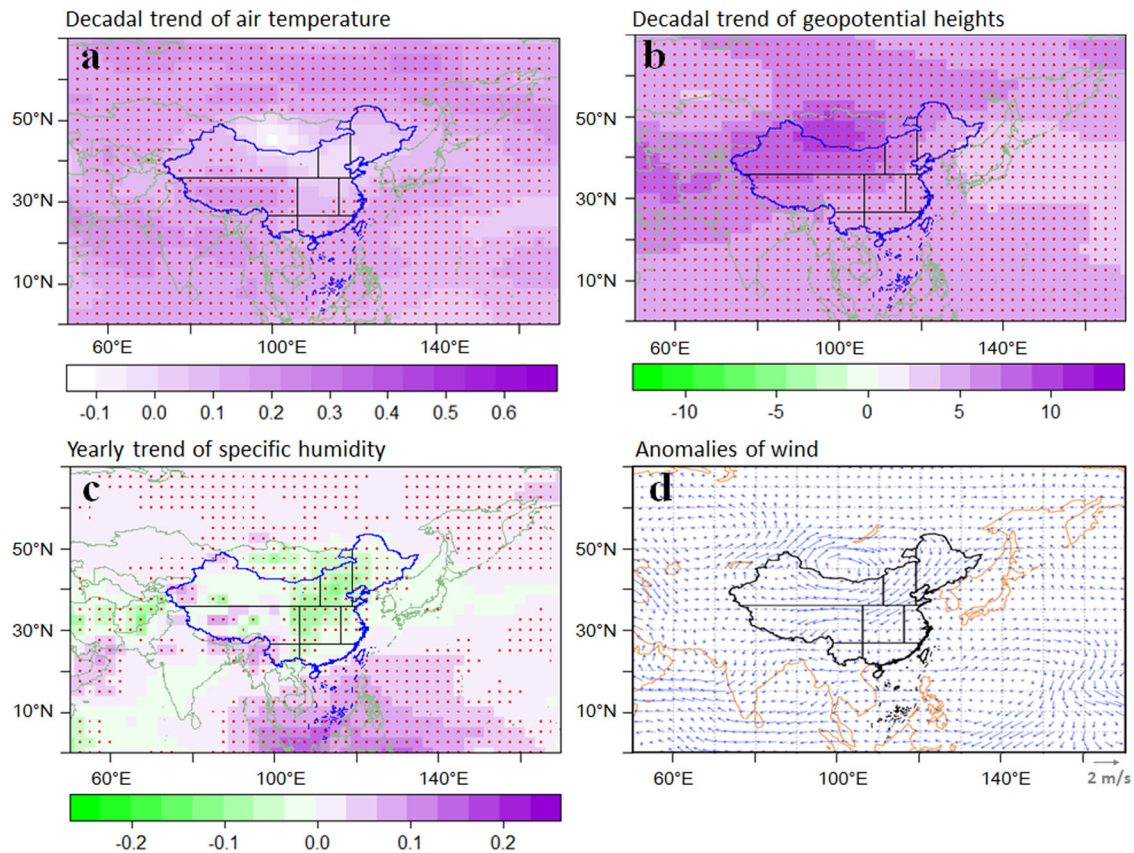
**Fig. 8 Maps of changes in the atmospheric variables.** Spatial distribution of the decadal trend of **a** air temperature and **b** geopotential height at 500 hPa from 1960 to 2018. **c** Spatial distribution of the yearly trend of specific humidity for 300–1000 hPa from 1960 to 2018. **d** The anomalies in wind at 500 hPa between the period 1991–2018 and 1960–1990. Areas with red dots indicate 95% significance. The subfigures were done in the software R 4.0.2 (https://cran.r-project.org/bin/windows/) and then the subfigures were merged by using the Microsoft PowerPoint 2013 software (https://www.microsoft.com/).

To conclude, based on the Gini-coefficients, this study has investigated the impacts of anthropogenic forcings on the temporal variability of annual precipitation extremes in China. The major findings of this study are summarized as follows: (1) although CMIPs simulations underestimate the Gini-coefficients in some regions of China, the overall magnitudes and spatial patterns of temporal variations for precipitation extremes are reasonably well characterized by a better performance of CMIP6; (2) a positive anthropogenic influence on the temporal variability of precipitation extremes has been clearly detected in China during the period 1961–2005; and (3) future projections of precipitation extremes (except for R95p) have a stepped upward trend over China, especially in southern China. Because precipitation extremes have significant implications for the net primary production of terrestrial ecosystems and agricultural yields, results obtained from this study not only offer insights into the temporal variability of precipitation extremes but also help policy makers for managing water-related disasters. For example, detailed dam management strategies could be improved for drought mitigation in southwest China.

## METHODS

### GCM datasets

In this study, we use two sets of simulations (one historical experiment and one historicalNat experiment) of 15 CMIP5 GCMs (Table S1) and four sets of simulations (one historical experiment and three future emission scenarios) of 20 CMIP6 GCMs (Supplementary Table 2). In general, the historical experiment has been forced by observed atmospheric composition changes (reflecting both anthropogenic and natural sources) and the time-evolving land cover[58]. While the historicalNat experiment is run only with the time-dependent natural forcing (solar and volcanic aerosols), hence providing estimates of the Earth's climate without anthropogenic influences[58]. The future emission scenarios are the socioeconomic pathways (shared socioeconomic pathways, SSPs) in CMIP6, which contain SSP126 (sustainability), SSP370 (regional rivalry), and SSP585 (fossil-fueled development)[59], generally corresponding to the representative concentration pathways (RCPs) 2.6, 6.0, and 8.5 in CMIP5[60]. In this study, after evaluating the performance of temporal variability of precipitation extremes for both CMIP5 and CMIP6 historical simulations, we explored the impact of anthropogenic forcings on extreme precipitation temporal variability of precipitation based on CMIP5 simulations. Finally, the future change has been evaluated based on the CMIP6 simulations. In order to better compare with observed data, the time period of historical and historicalNat simulations are selected from 1961 to 2005, and the time period of future simulations are selected from 2050 to 2095.

### Observed dataset

In order to compare with the historical simulations, observed daily precipitation data from 1961 to 2005 for China are utilized, which has been produced by the National Climate Center, China Meteorological Administration[61], on the basis of 2416 weather monitoring stations (hereafter referred to as CN05, see Fig. S1). Figure S1 shows that the total number of stations decreases steadily from east to the west and from south to the north, especially is very scarce in Northwest China (NWC) and Southwest China-region 1 (SWC1). The CN05 grid dataset has been constructed by using the method of "anomaly approach" based on the gridded daily anomaly and the gridded climatology[62], the resolution of which is 0.5° × 0.5°. The CN05 dataset has been successfully applied to evaluate detailed changes in regional climate change in China and validate high-resolution climate model[38,61].

## Computation of climate indices and data processing

Based on the Gini-coefficient, we have presented an analysis of impacts from anthropogenic forcing to the temporal variability of precipitation amounts (PRCPTOT), intensity (SDII) and extremes (R95p and RX5day), and investigate future changes in temporal precipitation variability under three scenarios over China. Four climate indices including PRCPTOT, SDII, R95p, and RX5day (Supplementary Table 4) have been selected and computed on an annual basis for observation data, historical climate simulations, historicalNat climate simulations, and future climate simulations to analyze and estimate the anthropogenic contribution to the temporal variability of precipitation in China. These indices were developed by the "Expert Team on Climate Change Detection and Indices" (ETCCDI) (available at http://etccdi.pacificclimate.org/)[63] and have been widely used to improve a constant perspective on changes in climate and weather extremes[45,64]. PRCPTOT is defined as the total amount of precipitation on wet days (days with precipitation >1 mm). SDII is the annual precipitation intensity. R95p is a percentile-based index, which quantifies the exceedance rates over the 95th percentile derived from the reference period. RX5day is an absolute index and represents the maximum consecutive 5-day precipitation amount.

Due to different resolutions between CMIP (CMIP5 and CMIP6) and CN05 data, the performance of the CMIP5 and CMIP6 models in simulating those precipitation extremes was evaluated in China based on the resolution at 1° × 1°, and found that the CMIP5 and CMIP6 models are generally able to simulate precipitation extremes over China. Following their approach, a first-order conservative remapping procedure[65] has been applied to regrid the precipitation indices to a common grid of resolution 1° latitude × 1° longitude for China by using Climate Data Operators (https://code.mpimet.mpg.de/projects/cdo/). In order to fully elaborate on regional changes, we have divided China into eight regions including Northeast China (NEC), Northern China (NC), Eastern China (EC), Central China (CC), Southern China (SC), Southwest China-region 1 (SWC1), Southwest China-region 2 (SWC2), and Northwest China (NWC), according to administrative boundaries and societal and geographical conditions[66]. Of them, NEC has a temperate continental monsoon climate with distinct seasons, NWC mainly contains Xinjiang and Gansu provinces and has a semi-arid and arid climate, SWC1 mainly contains the Tibetan plateau with a higher elevation (generally >3000 m), and SWC2 mainly contains Yunnan province and is affected by both the Indian monsoon, the East Asian monsoon.

## Gini-coefficient

The Gini-coefficient (G) is a well-established method for evaluating equity of resource allocation, mostly known for its use in measuring inequality of income or wealth in economics, but also recently and frequently used to measure the inequalities of changes of hydrometeorological elements (e.g., discharges, precipitation, and so on) under climate change and human activities[24,43,67,68]. Therefore, G has been used to depict the human contribution to potential changes in temporal precipitation variability (i.e., increase in unevenness or disparity) and quantify the inequality in the annual temporal distribution of future precipitation extremes in China. The precipitation index (PRCPTOT, SDII, P95p, and RX5day) has been calculated for each year, sorted by ascending order, summed cumulatively, and then converted into a proportion of time expressed by $P_i (i = 1, \ldots, n)$ with $n = 5$. The value of G can be calculated by doubling the area between the Lorenz curve and the absolute equality line (1:1 line) (Supplementary Fig. 2), which can be mathematically described as

$$G = \frac{1}{n}\left(n + 1 - 2 * \left(\frac{\sum_{i=1}^{n}(n+1-i)*P_i}{\sum_{i=1}^{n}P_i}\right)\right) \qquad (1)$$

The value of G theoretically ranges from 0 to 1. $G = 0$ indicates a uniform distribution of the precipitation index throughout the years, which means that all values are the same; while $G = 1$ represents maximal nonuniformity or the largest disparity distribution of precipitation throughout the years, which may suggest the annual precipitation index occurs in a single year during the entire study period. In general, smaller values of the Gini-coefficient imply more equality in the temporal variation of the precipitation indices, and vice versa.

By calculation, there is a single value of Gini-coefficient for each grid in CMIP5, CMIP6, and CN05 datasets. For the regional Gini-coefficient, we have computed the average value of the gridded Gini-coefficients over the specified regions. Therefore, each region has a single value of Gini-coefficient for each CMIP5 and CMIP6 realization separately for the historical, historicalNat, and future emission scenarios. Then, to examine the performance in temporal variability of CMIP5 and CMIP6 GCMs' precipitation simulations in China, we have first compared the Gini-coefficient of the observed and simulated PRCPTOT, SDII, R95p, and RX5day for the period 1961–2005.

## Detection and attribution

Climate models have become the most powerful tool not only for predicting climate change but also for fully understanding it, which have been also widely utilized in the analysis of extreme events based on different model experiments with different forcing combinations[12]. Climate models could be conducted with and without anthropogenic influences in order to quantify the extent of anthropogenic or natural influences for climate change or extreme events. Based on the Gini-coefficient, likewise, Konapala et al.[24] has defined a relative anthropogenic index (RAI) to evaluate the relative difference between historical and HistoricalNat simulations, which is applied in this study. The value of RAI can be calculated as

$$RAI = \frac{G_{ALL} - G_{NAT}}{G_{ALL}} = 1 - \frac{G_{NAT}}{G_{ALL}} \qquad (2)$$

where $G_{ALL}$ is the Gini-coefficient of the anthropogenic plus natural forcing (ALL) historical precipitation simulations, and $G_{NAT}$ represents the Gini-coefficient of natural forcing only (NAT) historical precipitation simulations. A positive value of RAI means an increase in annual precipitation variability during the study time period, whereas a negative value of RAI represents a decrease in annual precipitation variability during the study time period due to anthropogenic forcing. For each region, the regional Gini-coefficient has been used to calculate the RAI by Eq. (2) by using the multi-model ensemble means of CMIP5 historical simulations.

Similarly, we have defined a relative future index (RFI) to evaluate the relative difference between historical and future simulations, which can be mathematically described as

$$RFI = \frac{G_{Future} - G_{Historical}}{G_{Future}} = 1 - \frac{G_{Historical}}{G_{Future}} \qquad (3)$$

where $G_{Future}$ represents the Gini-coefficient of the CMIP6 future precipitation simulations (SSP126, SSP370, and SSP585), and $G_{Historical}$ equals $G_{ALL}$ in this study, representing the Gini-coefficient of the anthropogenic plus natural forcing (ALL) historical precipitation simulations. For each region, the regional Gini-coefficient has been used to calculate the RFI by Eq. (3) by using the multi-model ensemble means of CMIP6 future simulations.

In order to estimate the uncertainty of the Gini-coefficients and RAI (RFI), the Bootstrapping resampling procedure[69] has been used to generate 10,000 subsamples from the 41 CMIP5 realizations and 85 CMIP6 realizations. Then the percentile bootstrap method[70] was applied to calculate the endpoints for 5 or 95% bootstrap confidence interval, which means the fifth percentile and 95th percentile RAI (RFI) values. Therefore, the distribution of 10,000 RAI (RFI) values represents the uncertainty associated with using different models and provides a basis for communicating RAI (RFI) ranges. Also, a positive RAI (RFI) median is statistically significant if its fifth percentile value is also positive, while a negative RAI (RFI) median is statistically significant if its 95th percentile value is also negative[71–73]. Hence, the RAI estimates the influence of anthropogenic forcings on the temporal variation along with its significance, and the RFI estimates future changes on the temporal variation along with its significance.

## REFERENCES

1. Seneviratne, S. I. et al. Changes in climate extremes and their impacts on the natural physical environment (Intergovernmental Panel on Climate Change (IPCC). https://www.ipcc.ch/site/assets/uploads/2018/03/SREX-Chap3_FINAL-1.pdf (2012).
2. Min, S., Zhang, X., Zwiers, F. W. & Hegerl, G. C. Human contribution to more-intense precipitation extremes. *Nature* **470**, 378–381 (2011).
3. Cramer, W., Yohe, G. & Field, C. B. Detection and attribution of observed impacts. In *Climate Change 2014: Impacts, Adaptation, and Vulnerability. Part A: Global and Sectoral Aspects. Contribution of Working Group II to the Fifth Assessment Report of the Intergovernmental Panel on Climate Change* **2014** 979–1037 (Cambridge University Press, 2014).
4. Sun, W., Min, K. & Chern, J. Numerical study of 1998 late summer flood in East Asia. *Asia-Pac. J. Atmos. Sci.* **47**, 123–135 (2011).
5. Webster, P. J., Toma, V. E. & Kim, H. M. Were the 2010 Pakistan floods predictable? *Geophys. Res. Lett.* **38**, L4806 (2011).
6. Komori, D. et al. Characteristics of the 2011 Chao Phraya River Flood in Central Thailand. *Hydrol. Res. Lett.* **6**, 41–46 (2012).
7. Marengo, J. A. et al. The drought of Amazonia in 2005. *J. Clim.* **21**, 495–516 (2008).
8. Lewis, S. L., Brando, P. M., Phillips, O. L., van der Heijden, G. M. & Nepstad, D. The 2010 Amazon drought. *Science* **331**, 554 (2011).
9. AghaKouchak, A., Cheng, L., Mazdiyasni, O. & Farahmand, A. Global warming and changes in risk of concurrent climate extremes: insights from the 2014 California drought. *Geophys. Res. Lett.* **41**, 8847–8852 (2014).
10. Van Loon, A. F. et al. Drought in the anthropocene. *Nat. Geosci.* **9**, 89 (2016).
11. Trenberth, K. E. Attribution of climate variations and trends to human influences and natural variability. *Wiley Interdiscip. Rev. Clim. Change* **2**, 925–930 (2011).
12. Stott, P. A. et al. Attribution of extreme weather and climate-related events. *Wiley Interdiscip. Rev. Clim. Change* **7**, 23–41 (2016).
13. Trenberth, K. E., Fasullo, J. T. & Shepherd, T. G. Attribution of climate extreme events. *Nat. Clim. Change* **5**, 725 (2015).
14. Otto, F. E. Attribution of weather and climate events. *Annu. Rev. Env. Resour.* **42**, 627–646 (2017).
15. Shepherd, T. G. A common framework for approaches to extreme event attribution. *Curr. Clim. Change Rep.* **2**, 28–38 (2016).
16. Liu, C. & Allan, R. P. Observed and simulated precipitation responses in wet and dry regions 1850-2100. *Environ. Res. Lett.* **8**, 034002 (2013).
17. Held, I. M. & Soden, B. J. Robust responses of the hydrological cycle to global warming. *J. Clim.* **19**, 5686–5699 (2006).
18. Chou, C., Tu, J. & Tan, P. Asymmetry of tropical precipitation change under global warming. *Geophys. Res. Lett.* **34**, L17708 (2007).
19. Chou, C. et al. Increase in the range between wet and dry season precipitation. *Nat. Geosci.* **6**, 263–267 (2013).
20. Greve, P. et al. Global assessment of trends in wetting and drying over land. *Nat. Geosci.* **7**, 716–721 (2014).
21. Chadwick, R., Boutle, I. & Martin, G. Spatial patterns of precipitation change in Cmip5: why the rich do not get richer in the tropics. *J. Clim.* **26**, 3803–3822 (2013).
22. Byrne, M. P. & O Gorman, P. A. The response of precipitation minus evapo-transpiration to climate warming: why the "wet-get-wetter, dry-get-drier" scaling does not hold over land. *J. Clim.* **28**, 357614736 (2015).
23. Cassou, C. et al. Decadal climate variability and predictability: challenges and opportunities. *B. Am. Meteorol. Soc.* **99**, 479–490 (2018).
24. Konapala, G., Mishra, A. & Leung, L. R. Changes in temporal variability of precipitation over land due to anthropogenic forcings. *Environ. Res. Lett.* **12**, 24009 (2017).
25. Taschetto, A. S. & England, M. H. El Nino Modoki impacts on Australian rainfall. *J. Clim.* **22**, 3167–3174 (2009).
26. Feng, J., Chen, W., Tam, C. Y. & Zhou, W. Different impacts of El Niño and El Niño Modoki on China rainfall in the decaying phases. *Int. J. Climatol.* **31**, 2091–2101 (2011).
27. Knutson, T. R. et al. Tropical cyclones and climate change. *Nat. Geosci.* **3**, 157–163 (2010).
28. Walsh, K. J. E., McInnes, K. L. & McBride, J. L. Climate change impacts on tropical cyclones and extreme sea levels in the South Pacific-a regional assessment. *Glob. Planet. Change* **80-81**, 149–164 (2011).
29. Paek, H., Yu, J. Y. & Qian, C. Why were the 2015/2016 and 1997/1998 extreme El Niños different? *Geophys. Res. Lett.* **44**, 1848–1856 (2017).
30. Chen, H. & Sun, J. Contribution of human influence to increased daily precipitation extremes over China. *Geophys. Res. Lett.* **44**, 2436–2444 (2017).
31. Wu, Y., Wu, S. Y., Wen, J., Xu, M. & Tan, J. Changing characteristics of precipitation in China during 1960-2012. *Int. J. Climatol.* **36**, 1387–1402 (2016).
32. Liu, B., Xu, M., Henderson, M. & Qi, Y. Observed trends of precipitation amount, frequency, and intensity in China, 1960–2000. *J. Geophys. Res. Atmos.* **110**, D08103 (2005).
33. Li, H., Chen, H. & Wang, H. Effects of anthropogenic activity emerging as intensified extreme precipitation over China. *J. Geophys. Res. Atmos.* **122**, 6899–6914 (2017).
34. Chou, J. et al. Changes in extreme climate events in rice-growing regions under different warming scenarios in China. *Front. Earth Sci.* **9**, 655128 (2021).
35. Almazroui, M. et al. Projected changes in climate extremes using Cmip6 simulations over Srex regions. *Earth Syst. Environ.* **5**, 481–497 (2021).
36. Zhou, B., Wen, Q. H., Xu, Y., Song, L. & Zhang, X. Projected changes in temperature and precipitation extremes in China by the Cmip5 multimodel ensembles. *J. Clim.* **27**, 6591–6611 (2014).
37. Bader, D. C. et al. *Climate Models: An Assessment of Strengths and Limitations* (Department of Energy, Office of Biological and Environmental Research, 2008).
38. Duan, W. et al. Evaluation and future projection of Chinese precipitation extremes using large ensemble high-resolution climate simulations. *J. Clim.* **32**, 2169–2183 (2019).
39. Zhou, B., Xu, Y., Wu, J., Dong, S. & Shi, Y. Changes in temperature and precipitation extreme indices over China: analysis of a high-resolution grid dataset. *Int. J. Climatol.* **36**, 1051–1066 (2016).
40. Liu, K. S. & Chan, J. C. Recent increase in extreme intensity of tropical cyclones making landfall in South China. *Clim. Dynam.* **55**, 1059–1074 (2020).
41. Lui, Y. S., Tam, C. & Lau, N. Future changes in Asian summer monsoon precipitation extremes as inferred from 20-Km Agcm simulations. *Clim. Dynam.* **52**, 1443–1459 (2019).
42. Li, Y. G., He, D., Hu, J. M. & Cao, J. Variability of extreme precipitation over Yunnan Province, China 1960-2012. *Int. J. Climatol.* **35**, 245–258 (2015).
43. Sun, Q., Miao, C. & Duan, Q. Changes in the spatial heterogeneity and annual distribution of observed precipitation across China. *J. Clim.* **30**, 9399–9416 (2017).
44. Wang, Q., Zhai, P. & Qin, D. New perspectives on "warming-wetting" trend in Xinjiang, China. *Adv. Clim. Change. Res.* **11**, 252–260 (2020).
45. Sillmann, J., Kharin, V. V., Zhang, X., Zwiers, F. W. & Bronaugh, D. Climate extremes indices in the Cmip5 multimodel ensemble: part 1. model evaluation in the present climate. *J. Geophys. Res. Atmos.* **118**, 1716–1733 (2013).
46. Myhre, G. & Shindell, D. Anthropogenic and natural radiative forcing. In *Climate Change 2013: The Physical Science Basis. Contribution of Working Group I to the Fifth Assessment Report of the Intergovernmental Panel On Climate Change* 659–740 (Cambridge Univ. Press, 2013).
47. Zhang, Q. et al. Trends and abrupt changes of precipitation maxima in the Pearl River Basin, China. *Atmos. Sci. Lett.* **10**, 132–144 (2009).
48. You, Q. et al. Changes in daily climate extremes in China and their connection to the large scale atmospheric circulation during 1961–2003. *Clim. Dynam.* **36**, 2399–2417 (2011).
49. Liu, M. et al. Is southwestern China experiencing more frequent precipitation extremes? *Environ. Res. Lett.* **9**, 64002 (2014).
50. Lau, W. K. & Kim, K. The 2010 Pakistan flood and Russian heat wave: teleconnection of hydrometeorological extremes. *J. Hydrometeorol.* **13**, 392–403 (2012).
51. Milrad, S. M., Gyakum, J. R. & Atallah, E. H. A meteorological analysis of the 2013 Alberta flood: antecedent large-scale flow pattern and synoptic-dynamic characteristics. *Mon. Weather Rev.* **143**, 2817–2841 (2015).
52. Black, E., Blackburn, M., Harrison, G., Hoskins, B. & Methven, J. Factors contributing to the summer 2003 European heatwave. *Weather* **59**, 217–223 (2004).
53. Freychet, N., Tett, S., Wang, J. & Hegerl, G. Summer heat waves over eastern China: dynamical processes and trend attribution. *Environ. Res. Lett.* **12**, 24015 (2017).
54. Sun, J. et al. Why has the inner Tibetan Plateau become wetter since the mid-1990s? *J. Clim.* **33**, 8507–8522 (2020).
55. Peng, D. & Zhou, T. Why was the arid and semiarid Northwest China getting wetter in the recent decades? *J. Geophys. Res. Atmos.* **122**, 9060–9075 (2017).
56. Luo, Y., Wu, M., Ren, F., Li, J. & Wong, W. Synoptic situations of extreme hourly precipitation over China. *J. Clim.* **29**, 8703–8719 (2016).
57. Chen, H. Projected change in extreme rainfall events in China by the end of the 21St century using Cmip5 models. *Chi. Sci. Bull.* **58**, 1462–1472 (2013).
58. Taylor, K. E., Stouffer, R. J. & Meehl, G. A. An overview of Cmip5 and the experiment design. *B. Am. Meteorol. Soc.* **93**, 485–498 (2012).
59. O'Neill, B. C. et al. The scenario model intercomparison project (Scenariomip) for Cmip6. *Geosci. Model Dev.* **9**, 3461–3482 (2016).
60. Van Vuuren, D. P. et al. The representative concentration pathways: an overview. *Clim. Change* **109**, 5 (2011).
61. Wu, J. & Gao, X. A gridded daily observation dataset over China region and comparison with the other datasets. *Chin. J. Geophys.* **56**, 1102–1111 (2013).

62. New, M., Hulme, M. & Jones, P. Representing twentieth-century space-time climate variability. Part Ii: development of 1901-96 monthly grids of terrestrial surface climate. *J. Clim.* **13**, 2217–2238 (2000).
63. Zhang, X. et al. Indices for monitoring changes in extremes based on daily temperature and precipitation data. *Wiley Interdiscip. Rev. Clim. Change* **2**, 851–870 (2011).
64. Duan, W. et al. Changes of precipitation amounts and extremes over Japan between 1901 and 2012 and their connection to climate indices. *Clim. Dynam.* **45**, 2273–2292 (2015).
65. Jones, P. W. First-and second-order conservative remapping schemes for grids in spherical coordinates. *Mon. Weather Rev.* **127**, 2204–2210 (1999).
66. National Report Committee. *China's National Assessment Report on Climate Change (in Chinese)* (Science Press, 2007).
67. Masaki, Y., Hanasaki, N., Takahashi, K. & Hijioka, Y. Global-scale analysis on future changes in flow regimes using Gini and Lorenz asymmetry coefficients. *Water Resour. Res.* **50**, 4054–4078 (2014).
68. Rajah, K. et al. Changes to the temporal distribution of daily precipitation. *Geophys. Res. Lett.* **41**, 8887–8894 (2014).
69. Efron, B. & Tibshirani, R. J. *An Introduction to the Bootstrap* (CRC Press, 1994).
70. Paciorek, C. J., Stone, D. A. & Wehner, M. F. Quantifying statistical uncertainty in the attribution of human influence on severe weather. *Weather Clim. Extrem.* **20**, 69–80 (2018).
71. Fischer, E. M. & Knutti, R. Anthropogenic contribution to global occurrence of heavy-precipitation and high-temperature extremes. *Nat. Clim. Change* **5**, 560 (2015).
72. Lewis, S. C. & Karoly, D. J. Anthropogenic contributions to Australia's record summer temperatures of 2013. *Geophys. Res. Lett.* **40**, 3705–3709 (2013).
73. Zou, S. et al. Attribution of changes in the trend and temporal non-uniformity of extreme precipitation events in Central Asia. *Sci. Rep.* **11**, 15032 (2021).

## AUTHOR CONTRIBUTIONS

W.D. and S.Z. designed the analysis. W.D., S.Z., N.C., N.S., and N.S. collected the data; W.D., S.Z., N.S., Y.C., N.S., Z.L., G.F., and B.Z. performed the analysis; W.D. and S.Z. wrote the first draft of the paper. All authors contributed to the interpretation of the results and to the writing of the paper.

## COMPETING INTERESTS

The authors declare no competing interests.

## ADDITIONAL INFORMATION

**Supplementary information** The online version contains supplementary material available at https://doi.org/10.1038/s41612-022-00255-5.

**Correspondence** and requests for materials should be addressed to Shan Zou or Yaning Chen.

**Reprints and permission information** is available at http://www.nature.com/reprints

**Publisher's note** Springer Nature remains neutral with regard to jurisdictional claims in published maps and institutional affiliations.